CEAS-GNC-2022-069

CEAS EuroGNC 2022
"Conference on Guidance, Navigation and Control"
3-5 May 2022 @ Technische Universität Berlin, Germany

Accurate tracking of highly dynamic airplane trajectories using incremental nonlinear dynamic inversion

Fabian Gücker PhD Researcher, Technische Universität Braunschweig, Institute of Flight Guidance, 38108, Braunschweig, Germany. f.guecker@tu-braunschweig.de

Yannic Beyer PhD Researcher, Technische Universität Braunschweig, Institute of Flight Guidance, 38108, Braunschweig, Germany. y.beyer@tu-braunschweig.de

Meiko Steen Senior Researcher, Technische Universität Braunschweig, Institute of Flight Guidance, 38108, Braunschweig, Germany. m.steen@tu-braunschweig.de

Peter Hecker Professor, Technische Universität Braunschweig, Institute of Flight Guidance, 38108, Braunschweig, Germany. p.hecker@tu-braunschweig.de

ABSTRACT

Applications like automated dynamic soaring in the atmospheric boundary layer demand high accuracy and robustness from the path following flight controller. This presents a challenge because dynamic soaring trajectories in the atmospheric boundary layer typically involve load factors of about 5 g as well as large bank angles. Therefore, this paper presents a novel model-based controller whose performance is investigated using a generic highly dynamic smooth flight path. The controller consists of two cascades: an outer loop position controller and an inner loop quaternion-based attitude controller both of relative degree two. Based on the given flight path, a modified Frenet-Serret frame is used to feed forward the ideal flight-path axis system to the attitude controller. This reduces the control effort of the position controller, which only has to command small attitude changes concerning the ideal flight-path axis system. Both the feedforward and the position controller rely on purely kinematic quantities to increase the robustness. The attitude controller includes direct lift control by symmetric aileron deflection and is based on the robust method of incremental nonlinear dynamic inversion with control allocation. In the numerical simulation, we show for a 1 kg motor glider that the proposed controller design achieves high tracking accuracy. In future work, the control performance and robustness should be compared with that of other control concepts and validation should take place in flight testing.

Keywords: Incremental Nonlinear Dynamic Inversion; Kinematic Trajectory Tracking & Control; Modified Frenet-Serret Frame, Quaternion Attitude Control

1 Introduction

In recent years, research in the field of dynamic soaring has made steady progress [1]. The good understanding of the principles of dynamic soaring as well as sufficiently miniaturized available components for sensor technology enable current research on transferring the principle to automated unmanned aerial vehicles (UAVs). Since the required trajectories are highly dynamic and cannot be decomposed into parts, a core aspect of the project is to design a controller that can follow an arbitrary flyable trajectory in 3D space [2]. In addition, a high degree of abstraction, robustness to model uncertainties, and guidance accuracy in the presence of large perturbations due to wind are design goals. For these requirements, incremental nonlinear dynamic inversion [3–5] has made significant progress in recent years, especially in the field of unmanned multicopters [6, 7], and is therefore a suitable control method because only the control effectiveness of all control surfaces as well as the inertia and mass of the aircraft need to be known. Many ways to follow a trajectory have been presented in the past, but most of them are based on tracking a kind of surrogate target, which is pushed ahead on the trajectory in a suitable way [8–10]. Although this method often yields very good results, the dynamics of this target must be designed using heuristic methods. A 2D planar use of the Frenet-Serret frame is shown in Ref. [11–13]. A 3D-Frenet-Serret frame was already used in previous works, which improved the tracking performance, but also uses a surrogate target [14, 15]. Also a modified version of Frenet-Serret frame was used by Ref. [16] but lack the consideration of gravity in the reference frame and using a low dynamic trajectory to prove their approach. An overview about path following control strategies is given in Ref. [17]. The reduction of cascaded loops is known to increase bandwidth, because there need to be a minimum of one time-scale separation. A well known control structure is the use of four control loops consisting of a position control, flight path control, attitude and angular rate control loop [18]. A promising concept which is also taken up in this work is the reduction to an outer loop which, based on the trajectory and the position controller, provides a reference attitude which is then followed by an inner attitude control loop and consists of only two cascades [19, 20].

1.1 Contributions

We make the following contributions:

- We present a modified version of the Frenet-Serret frame that considers the gravitational acceleration and serves as flight-path reference attitude.
- We present a lightweight flight-path / trajectory tracking controller structure with two cascades and only two controlled variables with relative degree of two each. The code is publicly available on Github.[1]
- In simulation, we demonstrate high performance of the control structure over a wide range of speeds, rapidly changing load factors from 0.5 g up to 4.5 g, high bank angles ±150 deg and implied adaptability to the current flight situation without adaptive terms, while maintaining very small position errors.

1.2 Organization

The aircrafts rigid body dynamics and the control task are described in section 2. The control approach with two cascades is shown in section 3. The outer loop is the trajectory tracking reference with position controller. The inner loop represents the quaternion-based attitude controller with incremental nonlinear dynamic inversion and control allocation. The last section 4 shows the validation of the proposed control structure with a motor glider of 1 kg mass and 1.8 m span in numerical simulation.

[1]Data available online at `https://github.com/iff-gsc/HighlyDynamicTrajectory-EuroGNC2022`. Retrieved April 8, 2022.

2 Problem Formulation

2.1 Notation

We use the conventions of the international standard ISO 1151 in the area of flight dynamics. A lower-case subscript of a 3-D vector with the components x, y and z indicates that the vector is expressed in the corresponding frame. The inertial frame g is represented by the north-east-down coordinate system. The body frame b is originated at the center of gravity of the vehicle with forward-right-down convention. The air-path frame a is originated at the center of gravity of the vehicle, where x_a points in the direction of the airspeed vector. The flight-path frame k is originated at the center of gravity of the vehicle, where x_k points in the direction of the flight-path velocity. An upper-case subscript indicates relative motion of two frames: K indicates k relative to g. For symbols that are not part of ISO 1151, we use lower-case boldface symbols to denote vectors, upper-case boldface symbols for matrices and non-boldface symbols for scalars. The only exception are the three unit vectors $\boldsymbol{T}, \boldsymbol{B}, \boldsymbol{N}$, which form the orthonormal basis of the Frenet-Serret frame. The trajectory reference coordinate system t is originated at the center of gravity of the vehicle. Derivatives with respect to time are noted as usual with a dot above the variable $\dot{v}$. Derivatives of geometric functions according to the dimensionless parameter $t \in [0, 1]$ are noted with a derivative stroke $f'(t)$. Quaternions are noted with the scalar first convention $\boldsymbol{q} = [q_0\ q_1\ q_2\ q_3]^T$. So q_0 is the scalar part and q_1, q_2 and q_3 form the vector part.

2.2 Airplane Flight Dynamics

2.2.1 Equations of Motion

The six degrees of freedom rigid body equations of motion are applied to compute the angular velocity $\boldsymbol{\Omega}$, the attitude quaternion $\boldsymbol{q}_{bg}$, the velocity $\boldsymbol{V}_K$ and the position $\boldsymbol{s}_g = [x\ y\ z]^T$, with the mass m, the inertia matrix $\boldsymbol{I}_b$, the force $\boldsymbol{R}_b$, the moment $\boldsymbol{Q}_b$, the gravitational acceleration $g = 9.81\,\mathrm{m/s^2}$, $\boldsymbol{\Omega}_b = [p\ q\ r]^T$ and the rotation matrix from inertial to body frame $\boldsymbol{T}_{bg} = \boldsymbol{T}_{gb}^T = \boldsymbol{T}(\boldsymbol{q})$, see Eq. (35) and Ref. [21] section 1.7:

$$\dot{\boldsymbol{\Omega}}_b = \boldsymbol{I}_b^{-1} \left[\boldsymbol{Q}_b - \boldsymbol{\Omega}_b \times (\boldsymbol{I}_b\, \boldsymbol{\Omega}_b) \right] , \tag{1a}$$

$$\dot{\boldsymbol{q}}_{bg} = \frac{1}{2} \boldsymbol{q}_{bg} \otimes \begin{bmatrix} 0 & p & q & r \end{bmatrix}^T , \tag{1b}$$

$$\dot{\boldsymbol{V}}_{Kb} = \frac{1}{m} \boldsymbol{R}_b + \boldsymbol{T}_{bg} \begin{bmatrix} 0 & 0 & g \end{bmatrix}^T - \boldsymbol{\Omega}_b \times \boldsymbol{V}_{Kb} , \tag{1c}$$

$$\dot{\boldsymbol{s}}_g = \boldsymbol{T}_{gb}\, \boldsymbol{V}_{Kb} . \tag{1d}$$

2.2.2 Aerodynamics

The aerodynamics model is based on [21], Eq. (2.3-8b). The linear aerodynamic coefficients using derivatives, but considers the nonlinear axis transformation to convert the aerodynamic forces into the body frame, see Eq. (2). For the axis transformation, the rotation matrix is used, which depends on the angle of attack α and the angle of sideslip β, see Eq. (3).

$$\boldsymbol{R}_b^A = \boldsymbol{T}_{ba}\, \boldsymbol{R}_a^A \qquad\qquad \boldsymbol{Q}_b^A = \boldsymbol{T}_{ba}\, \boldsymbol{Q}_a^A \tag{2}$$

$$\boldsymbol{T}_{ba} = \begin{bmatrix} \cos\alpha\cos\beta & -\cos\alpha\sin\beta & -\sin\alpha \\ \sin\beta & \cos\beta & 0 \\ \sin\alpha\cos\beta & -\sin\alpha\sin\beta & \cos\alpha \end{bmatrix} \quad \text{with} \quad \begin{matrix} \alpha = \arctan\left(w_b/u_b\right) \\ \beta = \arcsin\left(v_b/V\right) \end{matrix} \tag{3}$$

The airspeed $V = \|\boldsymbol{V}\|$ takes into account the wind velocity $\boldsymbol{V}_W$. $\boldsymbol{V} = [u\ v\ w]^T = \boldsymbol{V}_K - \boldsymbol{V}_W$. The airframe force and moment vector are computed from the aerodynamic coefficients $C_{()}$ in the aerodynamic frame, see Eq. (4), where b is the span, c is the mean aerodynamic chord, S is the main wing area and $\rho = 1.225\,\mathrm{kg/m^3}$ is the air density.

$$\boldsymbol{R}_a^A = \frac{1}{2}\rho V^2 S \begin{bmatrix} C_{Xa} & C_{Ya} & C_{Za} \end{bmatrix}^T \qquad \boldsymbol{Q}_a^A = \frac{1}{2}\rho V^2 S \begin{bmatrix} b\,C_{la} & c\,C_{ma} & b\,C_{na} \end{bmatrix}^T \tag{4}$$

The aerodynamics coefficients include nonlinearities to account for the quadratic drag polar as well as stall. However, in this application the drag barely influences the controller performance and stall is avoided. That is why the aerodynamic coefficients can be approximated as a linear function:

$$\boldsymbol{c} = \boldsymbol{c}_0 + \frac{\partial \boldsymbol{c}}{\partial \boldsymbol{y}_{\text{Aero}}} \cdot \boldsymbol{y}_{\text{Aero}}\,, \tag{5}$$

where $\boldsymbol{c}$ comprises all aerodynamic coefficients:

$$\boldsymbol{c} = \begin{bmatrix} C_{Xa} & C_{Ya} & C_{Za} & C_{la} & C_{ma} & C_{na} \end{bmatrix}^T\,, \tag{6}$$

$\boldsymbol{c}_0$ are the aerodynamic coefficients in steady cruise flight and $\boldsymbol{y}_{\text{Aero}}$ comprises the main influence variables on the aerodynamic coefficients:

$$\boldsymbol{y}_{\text{Aero}} = \begin{bmatrix} \alpha & \beta & p^* & q^* & r^* & \xi_l & \xi_r & \eta & \zeta \end{bmatrix}^T \tag{7}$$

with normalized rate of roll $p^* = pb/V$, normalized rate of pitch $q^* = qc/V$, normalized rate of yaw $r^* = rb/V$, left and right aileron deflection angles ξ_l, ξ_r, elevator deflection angle η and rudder deflection angle ζ. The main influence variables do not include unsteady variables like $\dot{\alpha}$ for simplicity.

2.2.3 Actuator Dynamics

Second order delays including saturations of the states are used to model the actuator dynamics of the control surfaces. We note d_{act} as the damping ratio, ω_{act} is the angular frequency and $\delta_{\min} \le \delta \le \delta_{\max}$ and $\dot{\delta}_{\min} \le \dot{\delta} \le \dot{\delta}_{\max}$. Here, the symbol δ is representative for all actuator deflections ξ_l, ξ_r, η and ζ. The transfer function of the actuator is $A(s)$. The transfer function of the actuator model used for the INDI control loop is noted as $A'(s)$.

$$\ddot{\delta} = \omega_{\text{act}}^2 \left(\delta_{\text{cmd}} - \frac{2 d_{\text{act}}}{\omega_{\text{act}}} \dot{\delta} - \delta \right) \tag{8}$$

2.3 Control Objective

The control objective is that the aircraft position $\boldsymbol{s}$ follows the specified smooth flight path with as little error as possible. The reference position $\boldsymbol{r}$ required for this is the point on the flight path that is closest to the aircraft position. The aircraft should move along the flight path at a given speed. The corresponding speed controller is designed separately from the path following controller and is not discussed further in this paper.

3 Control Approach

The overall design of tracking high dynamic trajectories is divided into five simple sub-problems, see Fig. 1. The first step is calculating analytical expressions for the trajectory for each segment between given way-points. In the simplest form, these can be polynomials of any degree. However, care should be taken that they are sufficiently differentiable to ensure smooth trajectories. In this work, we use fifth-degree polynomials. The core of the highly dynamic control is the trajectory tracking and the calculation of the reference variables, see section 3.1. This is not done via heading and flight path angle independent of the flight condition, as it is often used in aviation [2, 19]. We use purely kinematic variables, which are calculated as a function of the current flight speed. The advantage of this calculation is that it does not require any information about the aircraft itself and can therefore be used universally for any type of aircraft, as stated in [19, 20]. To be as independent as possible from the actual aircraft, an inversion controller is used as the position controller, which is also based on purely kinematic variables, see section 3.2. However, a distinction must be made between the vertical and lateral positions for the reference position. These two differ concerning their connection to the rotational dynamics. For flying highly dynamic trajectories without limitations, it is necessary to have a reliable attitude controller for any flight condition. Therefore it is obvious to use a quaternion-based controller [6]. The attitude controller is based on incremental nonlinear dynamic inversion, see section 3.3 [22]. By feedback of the rotational accelerations, and explicit consideration of the actuator dynamics and feedback delay by filters, the highest possible bandwidth and robustness is ensured [23, 24]. The thrust controller is designed as a airspeed controller and ensures that the critical stall speed is not undershot at any time. This is designed as a simple PD controller and will not be discussed further in this paper. Since the aircraft used is a powered glider, which has only low climb performance. For aircraft with a high thrust-to-weight ratio, a model-based thrust control could also be used here, which compares the measured acceleration with a given reference. Without thrust control, trajectory control is simplified to path following control.

$$H(s) = \frac{\omega_n^2}{s^2 + 2\zeta\omega_n s + \omega_n^2} \tag{9}$$

The angular acceleration $\dot{\boldsymbol{\Omega}}_{b,\mathrm{f}}$ is obtained by differentiation of the gyroscope measurement. Because of expected noise amplification through the differentiation of the noisy measurement, the gyro signal is filterd by a second order filter based on Ref. [23, 25]. The same filtering is also applied to the accelerometer measurements as well as the aircraft position and the attitude. For the filter constants we choose $\omega_n = 50\,\mathrm{rad/s}$ and $\zeta = 0.55$ as suggested by Ref. [23].

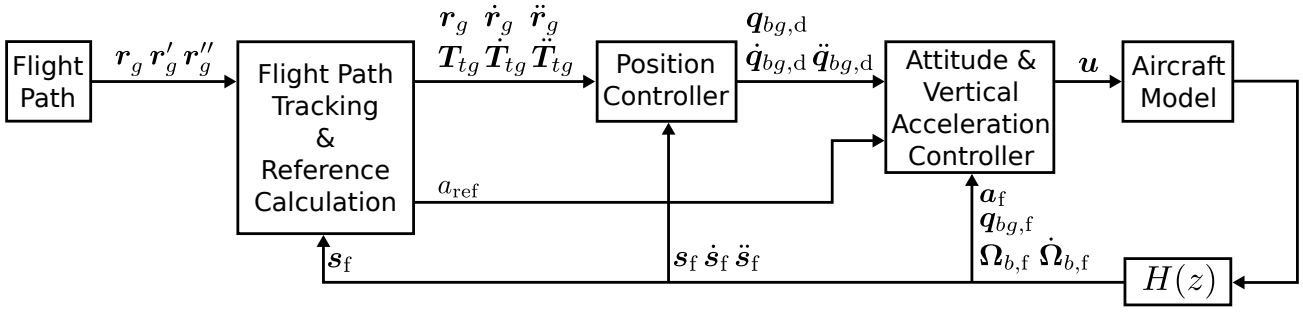

Fig. 1 Overall Controller Design

3.1 Trajectory tracking and attitude reference

First, the position t_m on the trajectory $\boldsymbol{r}_g(t)$ is determined which has the shortest distance to the current position of the aircraft. For this work, the shortest distance was determined by numerically calculating the zeros of the function given in Eq. (10). The trajectory is given by three polynomials

$f_x(t)$, $f_y(t)$ and $f_z(t)$ of degree 5. The filtered position is $\boldsymbol{s}_\mathrm{f} = [x_\mathrm{f}\ y_\mathrm{f}\ z_\mathrm{f}]$, see Fig. 1.

$$t_m = \underset{t\in[0,1]}{\arg\min} \left((f_x(t) - x_\mathrm{f})^2 + (f_y(t) - y_\mathrm{f})^2 + (f_z(t) - z_\mathrm{f})^2 \right) \tag{10}$$

As the result of the minimization problem, the dimensionless parameter t_m (matching) is obtained. In the next step, the derivatives of the matched trajectory position for the three spatial directions are determined for the current time step, see Eq.(11) and Fig. 2a.

$$\boldsymbol{r}_g(t_m) = \begin{bmatrix} f_x(t_m) \\ f_y(t_m) \\ f_z(t_m) \end{bmatrix} \qquad \boldsymbol{r}'_g(t_m) = \begin{bmatrix} f'_x(t_m) \\ f'_y(t_m) \\ f'_z(t_m) \end{bmatrix} \qquad \boldsymbol{r}''_g(t_m) = \begin{bmatrix} f''_x(t_m) \\ f''_y(t_m) \\ f''_z(t_m) \end{bmatrix} \tag{11}$$

With $\boldsymbol{r}_g$ and the first two derivatives $\boldsymbol{r}'_g$ and $\boldsymbol{r}''_g$ in respect to the dimensionless parameter t the so called Frenet-Serret frame can be calculated, see Fig. 2a. The Frenet-Serret frame consists of the tangent vector $\boldsymbol{T}$, the binormal vector $\boldsymbol{B}$ and the normal vector $\boldsymbol{N}$. The tangent vector $\boldsymbol{T}$ always points in the direction of the desired flight path and thus provides the reference for the direction of the flight-path velocity $V_K = \|\boldsymbol{V}_K\|$ and the x axis of the flight-path frame. The normal vector $\boldsymbol{N}$ points in the direction of the curvature κ of the path in the current point. A derivation of the Frenet-Serret frame and formulas is given in Ref. [26, 27]. Because the Frenet-Serret frame is a pure kinematic concept we need a way to include the gravitational acceleration to get an usable attitude reference:

$$\tilde{\boldsymbol{r}}''_g(t_m) = \begin{bmatrix} f''_x(t_m) \\ f''_y(t_m) \\ f''_z(t_m) - \frac{g}{v_t^2} \end{bmatrix} \tag{12}$$

To take into account the influence of gravitational acceleration g, we extend the second derivative $\boldsymbol{r}''$ by the additional term $-g/v_t^2$, as given in Eq. (12), where $v_t = \boldsymbol{V}_K \cdot \boldsymbol{T}$ is the component of the flight-path speed that is tangent to the desired flight path.

$$\boldsymbol{T}(t_m) = \frac{\boldsymbol{r}'_g(t_m)}{\left\|\boldsymbol{r}'_g(t_m)\right\|} \qquad \tilde{\boldsymbol{B}}(t_m) = \frac{\boldsymbol{r}'_g(t_m) \times \tilde{\boldsymbol{r}}''_g(t_m)}{\left\|\boldsymbol{r}'_g(t_m) \times \tilde{\boldsymbol{r}}''_g(t_m)\right\|} \tag{13}$$

Technically, with this step we increase the curvature of the path in the vertical direction in the inertial coordinate system. Practically, we increase the total curvature of the path and rotate the center of curvature along the tangent vector so that the modified normal vector $\tilde{\boldsymbol{N}}$ now corresponds to the vertical axis of the aircraft if the angle of attack is neglected. The modified binormal vector $\tilde{\boldsymbol{B}}$ points in the direction of the right wing to complete the orthonormal basis. This procedure is shown in Fig. 2b.

$$\tilde{\boldsymbol{N}}(t_m) = \tilde{\boldsymbol{B}}(t_m) \times \boldsymbol{T}(t_m) \qquad \kappa(t_m) = \frac{\left\|\boldsymbol{r}'_g(t_m) \times \tilde{\boldsymbol{r}}''_g(t_m)\right\|}{\left\|\boldsymbol{r}'_g(t_m)\right\|^3} \tag{14}$$

Together $\boldsymbol{T}$, $\tilde{\boldsymbol{B}}$ and $\tilde{\boldsymbol{N}}$ form the reference attitude a rigid body need to follow the trajectory with controllable acceleration along the vertical axis and body-fixed x-axis tangent to the path. The last missing information is the amount of this vertical acceleration, which can be easily determined from the trajectory curvature κ from Eq. (14) and the tangential velocity v_t according to Eq. (15):

$$\boldsymbol{a}_\mathrm{ref}(t_m) = \kappa(t_m)\, v_t^2(t_m) \tag{15}$$

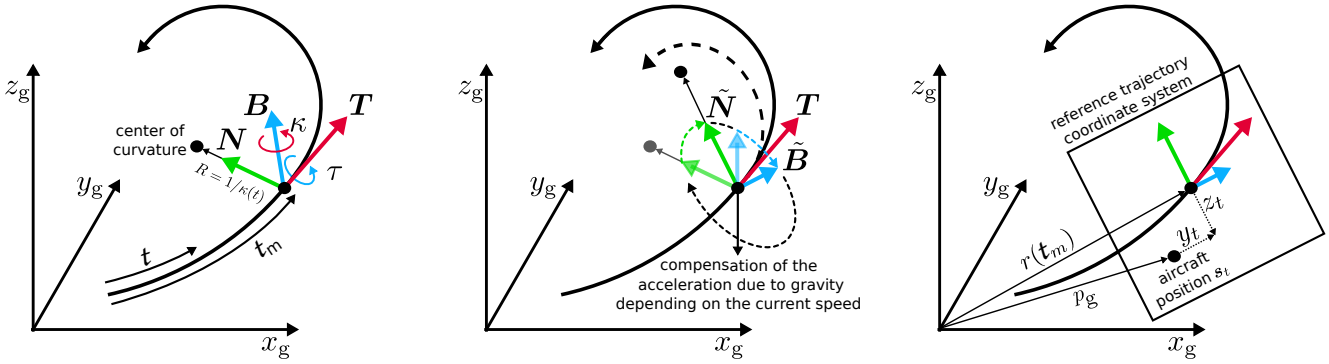

(a) Frenet-Serret frame with tangent vector T, normal vector N and binormal vector B. All are unit vectors.

(b) Modified Frenet-Serret frame by rotation around the tangent vector T. T, $\tilde{B}$ and $\tilde{N}$ form the flight-path reference system.

(c) Lateral position error y_t and vertical position error z_t in the reference trajectory coordinate system t which is axis-equivalent to the modified Frenet-Serret frame.

Fig. 2 Trajectory Tracking, Reference Attitude and Derivation of the Trajectory Coordinate System

At this point, a few things should be briefly highlighted. First, the presented method makes it very easy to determine a unique position reference that is free of singularities, assuming that the curvature κ is not zero. This rotation matrix $\boldsymbol{T}_{tg}$ can be formed directly from the modified Frenet-Serret frame as shown in Eq. (16). Note that the modified normal-vector $\tilde{\boldsymbol{N}}$ is reversed to match the axis orientation of the body-fixed system. Up to this point, no trigonometric functions have been used, making the approach numerically efficient.

$$\boldsymbol{T}_{tg} = \left[\boldsymbol{T}(t_m) \quad \tilde{\boldsymbol{B}}(t_m) \quad -\tilde{\boldsymbol{N}}(t_m)\right] \tag{16}$$

Furthermore, it should be mentioned that the correction term from Eq. (12) only twists the normal and binormal vector around the tangent vector. If the airplane flies only upward or downward, this term has no effect on the attitude. However, perhaps the most important property of this type of attitude reference can be quickly overlooked. By defining the attitude using a Frenet-Serret frame, the trajectory can be completely described by the curvature κ and torsion τ of the trajectory. The curvature corresponds to the pitch motion of the aircraft and the torsion to the roll motion. Thus, the reference flight-path sideslip angle is zero. Therefore, there is no need for a separate turn coordination as with other flight controllers. It should be noted that this only applies to the reference attitude. It does not apply to the actual attitude commanded by the subsequent controller or to a slip angle caused by the influence of wind. With the definiton of the flight-path (trajectory) reference system we need some additional angles. We define the flight path angles in trajectory coordinate system as $[\chi_t \quad \gamma_t \quad \mu_t]$. The angles from the trajectory to body-fixed system as $[\Phi_t \quad \Theta_t \quad \Psi_t]$ and the trajectory coordinate system t to body-fixed system b as $[x_t \quad y_t \quad z_t]$, see Fig. 2c.

3.2 Position Controller

The design of the two position controllers is based on model order reduction. The only question to be answered is, to which order can and must the reference model be reduced to obtain sufficient guidance accuracy and high error rejection. For both channels a controller with relative degree of two was chosen. This has shown in our simulations to be the one with the highest possible bandwidth as well as a great amount of robustness. The aim of the position controller is to control the aircraft position $\boldsymbol{s}_t$ in the

trajectory coordinate system, as well as its derivatives $\dot{\boldsymbol{s}}_t$ and $\ddot{\boldsymbol{s}}_t$ to zero.

$$\boldsymbol{s}_t = \boldsymbol{T}_{tg} \left(\boldsymbol{r}_g \left(t_m \right) - \boldsymbol{s}_\mathrm{f} \right) \tag{17a}$$

$$\dot{\boldsymbol{s}}_t = \boldsymbol{T}_{tg} \left(\dot{\boldsymbol{r}}_g \left(t_m \right) - \dot{\boldsymbol{s}}_\mathrm{f} \right) + \dot{\boldsymbol{T}}_{tg} \left(\boldsymbol{r}_g \left(t_m \right) - \boldsymbol{s}_\mathrm{f} \right) \tag{17b}$$

$$\ddot{\boldsymbol{s}}_t = \boldsymbol{T}_{tg} \left(\ddot{\boldsymbol{r}}_g \left(t_m \right) - \ddot{\boldsymbol{s}}_\mathrm{f} \right) + 2\,\dot{\boldsymbol{T}}_{tg} \left(\dot{\boldsymbol{r}}_g \left(t_m \right) - \dot{\boldsymbol{s}}_\mathrm{f} \right) + \ddot{\boldsymbol{T}}_{tg} \left(\boldsymbol{r}_g \left(t_m \right) - \boldsymbol{s}_\mathrm{f} \right) \tag{17c}$$

$$\boldsymbol{s}_t = \begin{bmatrix} x_t & y_t & z_t \end{bmatrix}^T \qquad \dot{\boldsymbol{s}}_t = \begin{bmatrix} \dot{x}_t & \dot{y}_t & \dot{z}_t \end{bmatrix}^T \qquad \ddot{\boldsymbol{s}}_t = \begin{bmatrix} \ddot{x}_t & \ddot{y}_t & \ddot{z}_t \end{bmatrix}^T \tag{17d}$$

3.2.1 Vertical Error Controller

From a purely kinematic point of view, the relationship between the vertical motion in the flight path reference system, the rotational dynamics given in Eq. (18) exists. This relationship for horizontal flight is sufficiently known from Ref. [19].

$$z_t = \int V_K\, \gamma_t\, \sin(\gamma_t) \tag{18a}$$

$$\dot{z}_t = V_K\, \sin(\gamma_t) \tag{18b}$$

$$\ddot{z}_t = V_K\, \sin(\gamma_t) + V_K\, \dot{\gamma}_t\, \cos(\gamma_t) \tag{18c}$$

On the assumption of small flight path angles γ_t and μ_t and the neglect of the angle of attack α, follows $\cos(\gamma_t) = 1$, $\sin(\gamma_t) = \gamma_t$. It should be mentioned that V_K must be limited to reasonable values above zero to prevent division by zero. The current velocity V_K, can be interpreted as the control effectiveness $\partial \dot{z}_t / \partial \gamma_t$ in Eq.(18b), for vertical motion in the trajectory reference system. The control law for the

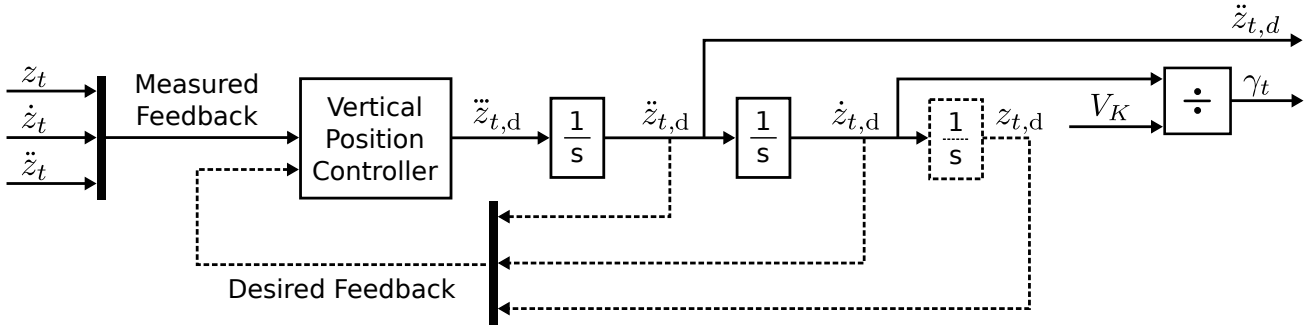

Fig. 3 Block diagram of the vertical position controller.

vertical position controller is given by Eq. (19). The gains are calculated to achieve the same response as a second-order closed-loop linear system, as shown in Fig.3 with the desired feedback path. Therefore, all poles are placed at $-\omega_V$.

$$\dddot{z}_{t,\mathrm{d}} = k_z\, z_t + k_{\dot{z}}\, \dot{z}_t + k_{\ddot{z}}\, \ddot{z}_t \tag{19}$$

The commanded path angle γ_t, that will be added to the reference attitude is obtained by integrating $\dddot{z}_{t,d}$ two times and then dividing by the current velocity V_K.

3.2.2 Lateral Error Controller

As before with vertical error control, the kinematic relationship between lateral motion and in stationary horizontal flight is investigated in Eq. (20). This time the lateral acceleration depends on the lateral orientation of the lift vector caused by a rotation around the longitudinal axis x_b of the airplane. This derivation is also based on the assumption of small angle of attack α, trajectory flight path angle γ_t

and small trajectory roll angle μ_t. The current vertical acceleration ng, can be interpreted as the control effectiveness $\partial \ddot{y}_t / \partial \mu_t$ in Eq. (20c), for lateral motion in the trajectory reference system.

$$y_t = \int \int n\, g\, \sin \mu_t \tag{20a}$$

$$\dot{y}_t = \int n\, g\, \sin \mu_t \tag{20b}$$

$$\ddot{y}_t = n\, g\, \sin \mu_t \tag{20c}$$

The control law for the lateral position controller is given by Eq. (21). The commanded flight path

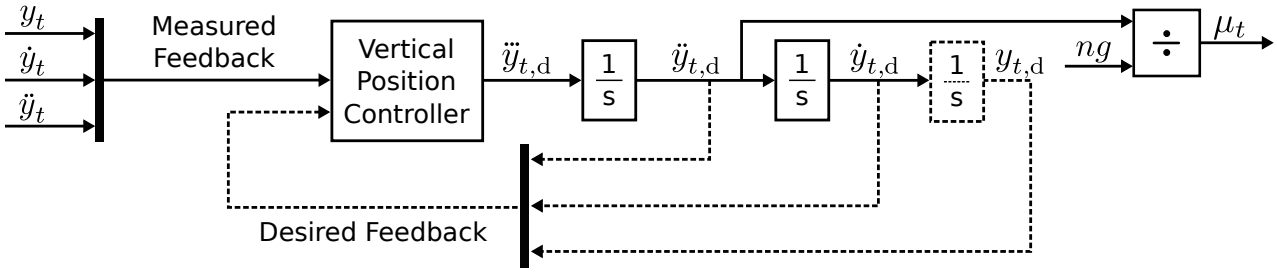

Fig. 4 Block diagram of the lateral position controller.

roll angle μ_t, that will be added to the flight path reference attitude $\boldsymbol{T}_{tg}$ is obtained by integrating $\ddot{y}_{t,d}$ and then dividing by the current trajectory normal acceleration that equals the load factor n times the acceleration due to gravity g, that is equal to a_{ref}. As in the vertical position controller, the gains are calculated to achieve the same response as a second-order closed-loop linear system, as shown in Fig.4 with the desired feedback path. Therefore, all poles are placed at $-\omega_L$.

$$\ddot{y}_{t,d} = k_y\, y_t + k_{\dot{y}}\, \dot{y}_t + k_{\ddot{y}}\, \ddot{y}_t \tag{21}$$

3.2.3 Position Controller Output Stage

After calculating the flight path angles for pitch γ_t and roll μ_t, the reference attitude given by the trajectory $\boldsymbol{T}_{tg}$ is rotated by these two angles. Please note, that these two angles are incremental values and no set of euler angles. The required step to take the flight path angles into account is to interpret them as a rotation vector. If small angles of incidence and sideslip are assumed, the path angles and body-fixed angles of rotation coincide in a good approximation. These then calculate the desired position in space which is transferred to the position controller, see Eq. (22).

$$\Theta_t \mathrel{\hat{=}} \gamma_t \qquad \Phi_t \mathrel{\hat{=}} \mu_t \tag{22}$$

This can be converted with the quaternion exponential into the necessary correction as a quaternion (23), that can be transferred into the necessary rotation matrix, see Eq.(24). Then the resulting desired attitude $\boldsymbol{T}_{bg,\mathrm{d}}$ is passed through a fast second order filter to smooth it and to generate consistent derivatives for the reference. Finally, the desired and filtered rotation matrix is converted into the command position quaternion $\boldsymbol{q}_{bg,\mathrm{d}}$. The required first $\dot{\boldsymbol{q}}_{bg,\mathrm{d}}$ and second derivative $\ddot{\boldsymbol{q}}_{bg,\mathrm{d}}$, can be calculated by numerical differentiation, this is possible, because the rotation matrix was filtered before and small rotations per time step are assumed. At this point it should be noted that filtering the rotation matrix result in a LERP like reference, for absolutely trustworthy reference calculation, the filtering should be done directly on a quaternion basis, but this is outside the focus of this work.

$$\boldsymbol{q}_{tk} = \exp\left(\begin{bmatrix} 0 & \Phi_t & \Theta_t & 0 \end{bmatrix}^T\right) \tag{23}$$

$$\boldsymbol{T}_{bg,\mathrm{d}} = \boldsymbol{T}_{tg}\,\boldsymbol{T}(\boldsymbol{q}_{tk})^T \tag{24}$$

3.3 Attitude and Vertical Acceleration Controller

The block diagram of the attitude controller is shown in Figure 5. The commanded attitude from position controller $\boldsymbol{q}_\mathrm{d}$ as well as its first two derivatives are the reference variables. The controlled variables are the measured attitude $\boldsymbol{q}_\mathrm{f}$, the rotational velocity in the body-fixed coordinate system $\Omega_{b,\mathrm{f}}$ and the rotational accelerations $\dot{\Omega}_{b,\mathrm{f}}$ determined from filtering the rotational velocity from the gyroscopes. The angular distance for each axis between the reference attitude $\boldsymbol{q}_\mathrm{d}$ and the current attitude $\boldsymbol{q}_\mathrm{f}$ of the

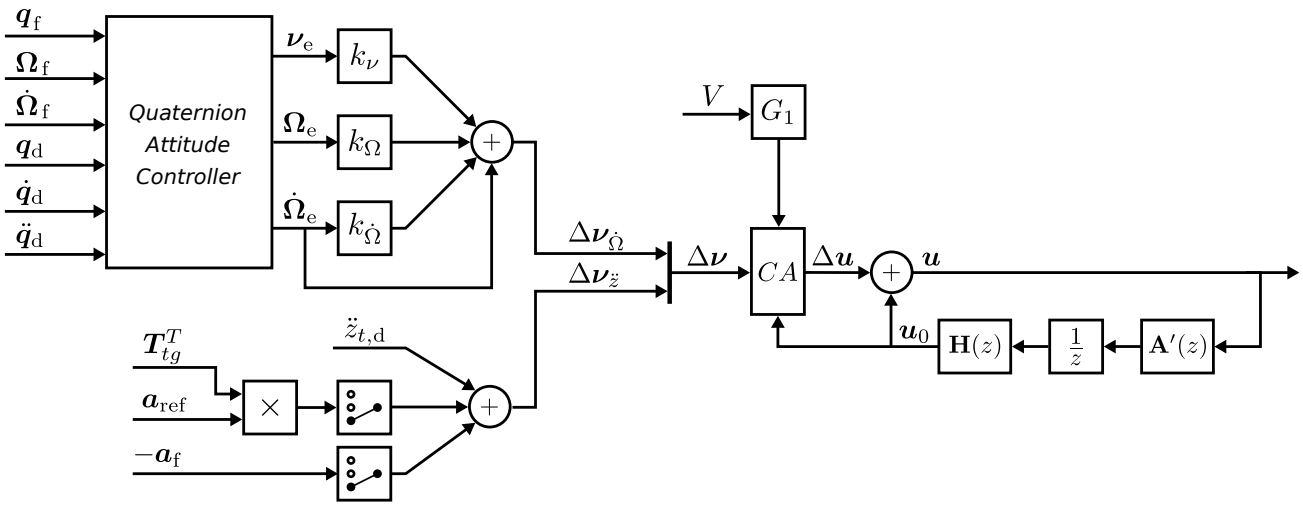

Fig. 5 Attitude and Vertical Acceleration Controller with Control Allocation and Incremental Nonlinear Dynamic Inversion

aircraft is given by Eq. (25). This result is known as the rotation vector representation. All quaternions and their derivatives transform form inertial into body-fixed coordinate system, for better readability the index $\boldsymbol{q}_{bg}$ is missing intentionally. $\boldsymbol{q}^{-1}$ note the inverse of a quaternion.

$$\boldsymbol{q}_\mathrm{e} = 2\ln\left(\boldsymbol{q}_\mathrm{f}^{-1} \otimes \boldsymbol{q}_\mathrm{d}\right) \tag{25}$$

The calculation of the error for the angular rates and the angular acceleration is done according to Eq. (26). With $\boldsymbol{q}^*$ we note the conjugate of a quaternion.

$$\boldsymbol{q}_\Omega = 2\left(\boldsymbol{q}_\mathrm{d}^* \otimes \dot{\boldsymbol{q}}_\mathrm{d}\right) \qquad \boldsymbol{q}_{\dot{\Omega}} = 2\left(\dot{\boldsymbol{q}}_\mathrm{d}^* \otimes \dot{\boldsymbol{q}}_\mathrm{d}\right) + 2\left(\boldsymbol{q}_\mathrm{d}^* \otimes \ddot{\boldsymbol{q}}_\mathrm{d}\right) \tag{26}$$

For the control law only the vector part of the quaternion is necessary:

$$\boldsymbol{\nu}_\mathrm{e} = \begin{bmatrix} q_{\mathrm{e},1} \\ q_{\mathrm{e},2} \\ q_{\mathrm{e},3} \end{bmatrix} \qquad \boldsymbol{\Omega}_\mathrm{e} = \begin{bmatrix} q_{\Omega,1} \\ q_{\Omega,2} \\ q_{\Omega,3} \end{bmatrix} - \boldsymbol{\Omega}_{b,\mathrm{f}} \qquad \dot{\boldsymbol{\Omega}}_\mathrm{e} = \begin{bmatrix} q_{\dot{\Omega},1} \\ q_{\dot{\Omega},2} \\ q_{\dot{\Omega},3} \end{bmatrix} - \dot{\boldsymbol{\Omega}}_{b,\mathrm{f}} \tag{27}$$

For unit quaternions the control law is given in Eq. (28). The first term in brackets contains the controller, the second term is the measured feedback for the incremental nonlinear dynamic inversion. This can be

irritating at first sight, because in the literature usually the reference acceleration, the measured rotational acceleration and the controller are connected to the last additions block. However, the calculation of the difference between reference and feedback is already done in the controller, see Eq. (27).

$$\Delta \boldsymbol{\nu}_{\dot{\Omega}} = \left(k_v \, \boldsymbol{v}_\mathrm{e} + k_\Omega \, \boldsymbol{\Omega}_\mathrm{e} + k_{\dot{\Omega}} \, \dot{\boldsymbol{\Omega}}_\mathrm{e}\right) + \dot{\boldsymbol{\Omega}}_\mathrm{e} \tag{28}$$

The pseudo-control part for the vertical acceleration is given in Eq. (29).

$$\Delta \boldsymbol{\nu}_{\ddot{z}} = \ddot{z}_{t,\mathrm{d}} + \begin{bmatrix} 0 & 0 & 1 \end{bmatrix} \left(\boldsymbol{T}_{tg}^T \, \boldsymbol{a}_\mathrm{ref} - \boldsymbol{a}_\mathrm{f}\right) \tag{29}$$

In the last step of the attitude controller, the commanded angular and vertical accelerations are multiplied by the control effectiveness of the control surfaces through the control allocation. The incremental nonlinear dynamic inversion receives the pseudo control $\Delta\boldsymbol{\nu}$ as reference. The actuator dynamics $\boldsymbol{A}'(z)$ are taken into account in the feedback of the INDI loop as well as the filter transfer function of the sensors $\boldsymbol{H}(z)$ as in Ref. [23]. The pseudo-control vector $\Delta\boldsymbol{\nu}$ is composed from the commanded angular acceleration vector and vertical acceleration, see. Eq. (30).

$$\Delta \boldsymbol{\nu} = \begin{bmatrix} \Delta \boldsymbol{\nu}_{\dot{\Omega}}^T & \Delta \boldsymbol{\nu}_{\ddot{z}} \end{bmatrix}^T \tag{30}$$

The available control surfaces are the left aileron ξ_l, right aileron ξ_r, elevator η and rudder ζ. They are limited to the range between -1 and 1 and thus limits the actuator deflection to the mechanically permissible values. The motor control is omitted at this point, since it has no influence on the position or vertical movement. The commanded actuator position vector $\boldsymbol{u}$ is given in Eq. (31).

$$\boldsymbol{u} = \begin{bmatrix} \xi_l & \xi_r & \eta & \zeta \end{bmatrix}^T \qquad \text{with} \quad \xi_l, \xi_r, \eta, \zeta \in [-1, 1] \tag{31}$$

We use the well known weightes least squares (WLS) algorithm which from Ref. [28]. Due to the incremental controller structure it is necessary to adapt the limits in each step to the current manipulated variable of the actuators $\boldsymbol{u}_0$, see Eq. (32) as suggested in Ref. [24].

$$\bar{\boldsymbol{u}}_\mathrm{min} = \boldsymbol{u}_\mathrm{min} - \boldsymbol{u}_0 \tag{32a}$$

$$\bar{\boldsymbol{u}}_\mathrm{max} = \boldsymbol{u}_\mathrm{max} - \boldsymbol{u}_0 \tag{32b}$$

$$\bar{\boldsymbol{u}}_\mathrm{d} = \boldsymbol{u}_\mathrm{d} - \boldsymbol{u}_0 \tag{32c}$$

After the adjustment, the actuator increment $\Delta\boldsymbol{u}$ can be resolved using the active set method.

$$\Delta \boldsymbol{u} = \underset{\bar{\boldsymbol{u}} \in [\bar{\boldsymbol{u}}_\mathrm{min}, \, \bar{\boldsymbol{u}}_\mathrm{max}]}{\arg\min} \left\| \begin{bmatrix} \gamma^{\frac{1}{2}} \boldsymbol{W}_\nu \boldsymbol{G} \\ \boldsymbol{W}_u \end{bmatrix} \bar{\boldsymbol{u}} - \begin{bmatrix} \gamma^{\frac{1}{2}} \boldsymbol{W}_\nu \boldsymbol{\nu} \\ \boldsymbol{W}_u \bar{\boldsymbol{u}}_\mathrm{d} \end{bmatrix} \right\|^2 \quad \text{with} \quad \bar{\boldsymbol{u}}_0 = \frac{1}{2} \left(\bar{\boldsymbol{u}}_\mathrm{min} + \bar{\boldsymbol{u}}_\mathrm{max}\right) \tag{33}$$

Finally, the actuator increment $\Delta\boldsymbol{u}$ is added to the actuator position $\boldsymbol{u}_0$ of the last time step.

$$\boldsymbol{u} = \Delta \boldsymbol{u} + \boldsymbol{u}_0 \tag{34}$$

4 Results

4.1 Simulation Setup

For the validation of the controller we use our own model of a generic motor glider with a mass of 1 kg and a wingspan of 1.8 m. A sketch of the used aircraft and the control surface layout is shown in Fig. 6. The further geometric data can be found in the appendix in Tab. 3. The same applies to the aerodynamic derivatives, see Tab. 3.

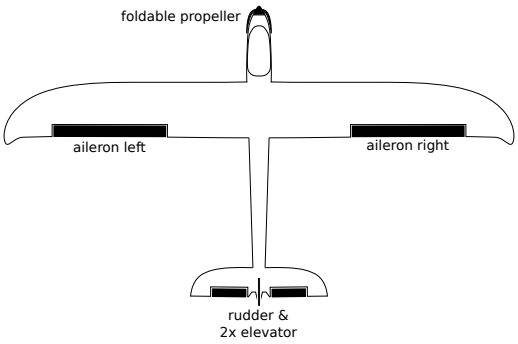

Fig. 6 Top view of the aircraft used for simulation. The control surfaces are highlighted in black and consist of two independently controllable ailerons, an elevator, a rudder and the propulsion system in the nose tip with a folding propeller.

4.2 Reference Tracking

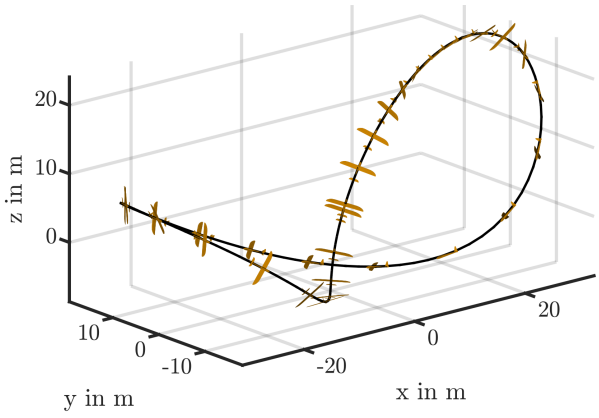

(a) First lap with low speed

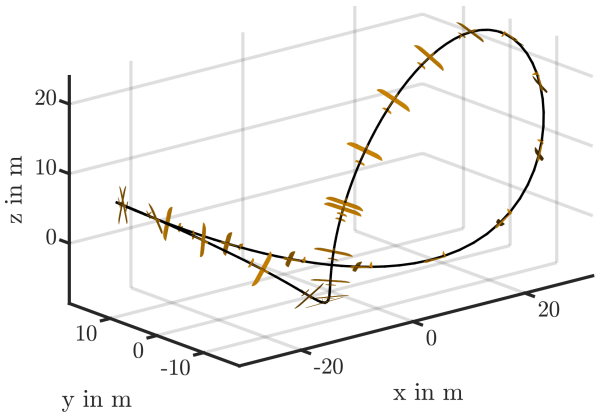

(b) Second lap with higher speed

Fig. 7 Aircraft trajectory from numerical simulation. The aircraft's attitude and position is shown for successive frames of one second delay each. The aircraft is shown three times larger to better see the orientation in space.

The first simulation will validate the guidance performance of the presented controller structure. The trajectory is a three-dimensional horizontal figure eight, which does not intersect itself, see Fig 7. As a special feature of the trajectory, the two ends of the trajectory are raised differently. The aircraft takes off trimmed from point A and flies two laps from there. At the beginning of the first lap flown with a very low setting of the thrust controller, so that the speed at the highest point of the trajectory is only 5 m/s with a bank angle of 20 deg. In the middle of the first lap, the thrust regulator is set to maximum. There is a significant increase in average speed. The next time the high point is reached, the speed is about 18 m/s and the bank angle is 150 deg. The two points with maximum altitude are marked with vertical yellow lines in Fig. 8-10. The load factor at this moment is about 1g. The position error is both vertically

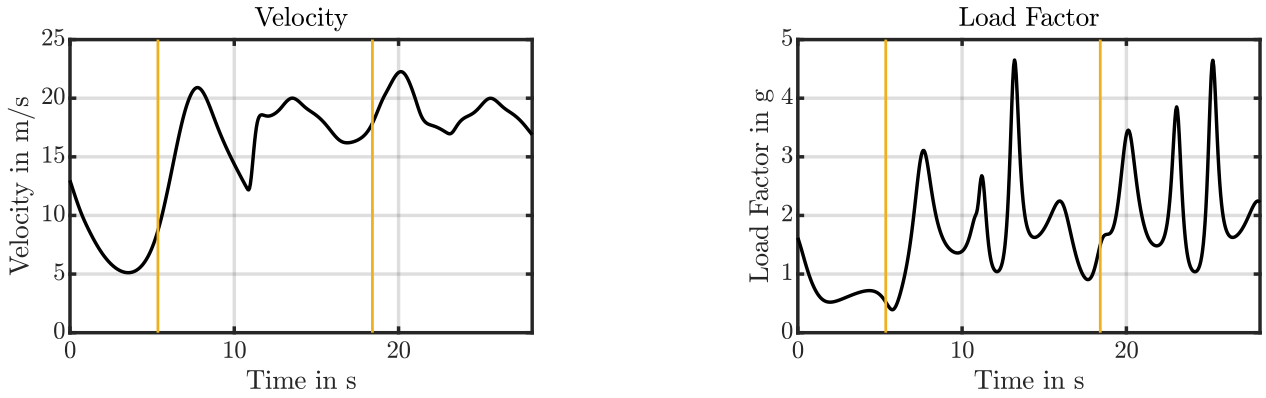

Fig. 8 Measured load factor and velocity from simulation for the reference flight path.

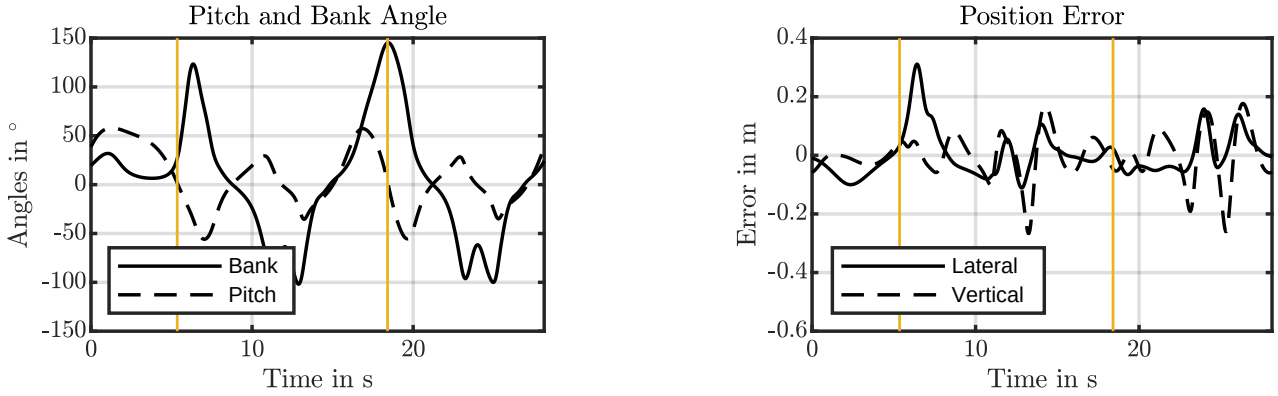

Fig. 9 Measured pitch angle, bank angle and position s_t from simulation for the reference flight path.

and laterally during both rounds in the range of ±0.3 m although a load factor up to 4.5 g and rapidly changing speeds in the range of 5 - 22 m/s, see Fig. 9. It should be remarked, that the stall speed of the usesd model is about 7 m/s and stall is only prevented by the low load factor 0.5 g at the moment of lowest velocity, see Fig. 8. During flight, aileron saturation occurs shortly after reaching the high point for the first time, see Fig. 10. Due to the lack of redundancy of control surfaces for the roll motion, this cannot be compensated in any other way by the control allocation. However, this is not a problem, because this saturation occurs mainly due to the low speed and the resulting low control effectiveness at this moment, as soon as the speed increases again, the two actuators go out of the limit again without chattering, see Fig. 10. The simulation shows that the presented controller structure is able to follow a highly dynamic trajectory with high accuracy even if the speed and resulting load factors vary strongly during the flight.

4.3 Error Dynamics

Fig. 11 shows the response of the position error in case of a inital position error of 2 m in vertical and lateral direction for straight and level flight with $V = 14\,\mathrm{m/s}$. The controller parameterization is the same as in the example above. The typical transient response of the desired linear second order system as well as the steady state accuracy can be seen. In addition, it can be seen that the speed of the position controller with $\omega_\mathrm{L} = 0.75\,\mathrm{rad/s}$ and $\omega_\mathrm{V} = 2.0\,\mathrm{rad/s}$ is chosen relatively slow.

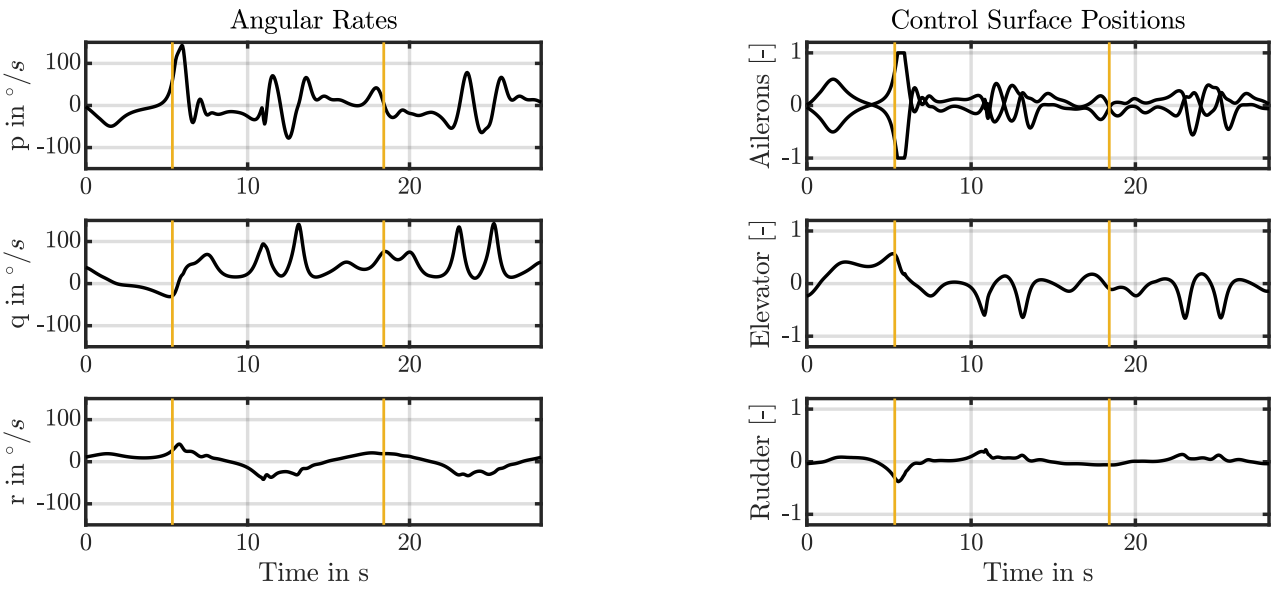

Fig. 10 Measured angular rates and actuator positions from simulation for the reference flight path.

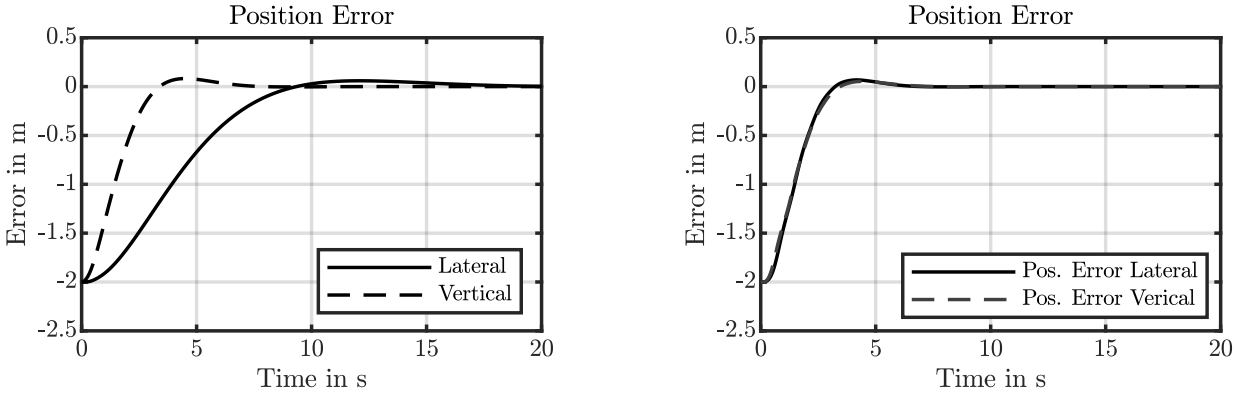

Fig. 11 System response to an initial deposit of 2 m in vertical and lateral direction during stationary straight flight. On the left, ω_V = 2.0 rad/s for the vertical channel and ω_L = 0.75 rad/s for the lateral direction was selected as the reference speed for the controller. Right for both channels with $\omega_{L,V}$ = 2.0 rad/s.

5 Conclusion

In this work, a controller concept was presented which consists of only two cascades and is based purely on kinematic relationships up to the last inner cascade of the position controller. For the design of the whole controller structure three single controllers with pole placement are determined. This procedure can be automated very well and corresponding safeties can be included. By feeding back the rotational acceleration in the INDI control loop, model uncertainties are compensated for as far as possible and thus only the three control efficiencies of the three degrees of roll freedom are required. However, high potential can already be assumed at this point, since the approach is very easy to parameterize and only three time constants can be used to parameterize the controller. The other variables needed for the inner loop are all model based and dependent on the corresponding aircraft. Namely, actuator dynamics and control effectiveness. Due to the open integrators of the reference model in the position controller, both the lateral and the vertical are stationary accurate, but without catching an additional pole point with its own dynamics as with an I-controller. In the future, this control approach will be extensively compared with those in the literature to rank its performance and especially robustness.

Appendix

Quaternion Math

Transformation matrix from a quaternion:

$$\boldsymbol{T}(\boldsymbol{q}) = \begin{bmatrix} 1-2q_2^2-2q_3^2 & 2q_1q_2-2q_0q_3 & 2q_1q_3+2q_0q_2 \\ 2q_1q_2+2q_0q_3 & 1-2q_1^2-2q_3^2 & 2q_2q_3-2q_0q_1 \\ 2q_1q_3-2q_0q_2 & 2q_2q_3+2q_0q_1 & 1-2q_1^2-2q_2^2 \end{bmatrix} \tag{35}$$

Quaternion multiplication:

$$\boldsymbol{p} \otimes \boldsymbol{q} = \begin{bmatrix} p_0q_0 - p_1q_1 - p_2q_2 - p_3q_3 \\ p_0q_1 + p_1q_0 + p_2q_3 - p_3q_2 \\ p_0q_2 - p_1q_3 + p_2q_0 + p_3q_1 \\ p_0q_3 + p_1q_2 - p_2q_1 + p_3q_0 \end{bmatrix} = \begin{bmatrix} q_0 & -q_1 & -q_2 & -q_3 \\ q_1 & q_0 & q_3 & -q_2 \\ q_2 & -q_3 & q_0 & q_1 \\ q_3 & q_2 & -q_1 & q_0 \end{bmatrix} \begin{bmatrix} p_0 \\ p_1 \\ p_2 \\ p_3 \end{bmatrix} \tag{36}$$

Controller parameters

Table 1 Feedback gain settings of the position and attitude controller.

Parameter	k_ν	k_Ω	$k_{\dot{\Omega}}$	k_z	$k_{\dot{z}}$	$k_{\ddot{z}}$	k_y	$k_{\dot{y}}$	$k_{\ddot{y}}$
Value	$45.0\,\mathrm{s}^{-2}$	$13.5\,\mathrm{s}^{-1}$	0.35	$8.0\,\mathrm{s}^{-2}$	$12.0\,\mathrm{s}^{-1}$	6.0	$1.0\,\mathrm{s}^{-2}$	$3.0\,\mathrm{s}^{-1}$	3.0

Natural frequencies for the reference generation of gyro and acceleratormeter and the attitude reference for the inner INDI loop:

$$\omega_\mathrm{f} = 50\,\mathrm{rad/s} \qquad D_\mathrm{f} = 0.55 \tag{37a}$$
$$\omega_\mathrm{atti} = 12\,\mathrm{rad/s} \qquad D_\mathrm{atti} = 1 \tag{37b}$$
$$\omega_\mathrm{V} = 1.5\,\mathrm{rad/s} \qquad D_\mathrm{V} = 1 \tag{37c}$$
$$\omega_\mathrm{L} = 1.0\,\mathrm{rad/s} \qquad D_\mathrm{L} = 1 \tag{37d}$$

Parameters for control allocation:

$$\boldsymbol{W}_\nu = \mathrm{diag}\,(10,\ 10,\ 10,\ 1) \qquad \boldsymbol{W}_u = \mathrm{diag}\,(1\mathrm{e}4,\ 1\mathrm{e}4,\ 1,\ 1) \tag{38a}$$
$$\boldsymbol{u}_\mathrm{min} = \begin{bmatrix} -1 & -1 & -1 & -1 \end{bmatrix}^T \qquad \boldsymbol{u}_\mathrm{max} = \begin{bmatrix} 1 & 1 & 1 & 1 \end{bmatrix}^T \tag{38b}$$
$$\boldsymbol{u}_\mathrm{d} = \begin{bmatrix} 0.0 & 0.0 & 0.0 & 0.0 \end{bmatrix}^T \qquad \gamma = 1\mathrm{e}6 \tag{38c}$$

Control effectiveness at 14 m/s trim speed:

$$\left.\frac{\partial \boldsymbol{\nu}}{\partial \boldsymbol{u}}\right|_{u_0} = \begin{bmatrix} 47.675 & -47.675 & 0 & 0 \\ -19.635 & -19.635 & 59.530 & 0 \\ 0 & 0 & 0 & 17.660 \\ -17.400 & -17.400 & 4.178 & 0 \end{bmatrix}, \qquad \boldsymbol{u}_0 = \begin{bmatrix} 0.0 & 0.0 & 0.0 & 0.0 \end{bmatrix}^T \tag{39}$$

Airplane parameters

Table 2 Compilation of the aerodynamic derivatives of the motor glider model, where $\partial C_{Za}/\partial\alpha$ is the field at row C_{Za} and column α. The geometric references are $S = 0.3358\,\mathrm{m}^2$, $c = 0.185\,\mathrm{m}$ and $b = 1.815\,\mathrm{m}$.

	α	β	p^*	q^*	r^*	$\xi_{\mathrm{l,r}}$	η	ζ	trim
C_{Xa}	-0.109	-0.001	0	-0.096	0.001	0	0.004	0.001	-0.049
C_{Ya}	0	-0.328	-0.001	0	0.111	0	0	-0.076	0
C_{Za}	-5.708	0	0	-4.02	0	0	0.102	0	-0.238
C_{la}	0	-0.007	-0.241	-0.001	0.034	0.091	0	0	0
C_{ma}	-2.048	0	0	-7.956	0	0	0.379	0	0
C_{na}	0	0.104	0.004	0	-0.045	-0.005	0	0.029	0

Table 3 Rigid body and actuator parameters of the simulation model.

Symbol	Value	Unit	Symbol	Value	Unit
m	1.0	kg	ω_{act}	80	rad/s
I_x	0.0712	$\mathrm{kg\,m^2}$	d_{act}	1	-
I_y	0.0482	$\mathrm{kg\,m^2}$	$\delta_{\max}$	15	°
I_z	0.1182	$\mathrm{kg\,m^2}$	$\delta_{\min}$	−15	°
I_{xy}, I_{zx}, I_{yz}	-	$\mathrm{kg\,m^2}$	$\dot{\delta}_{\max}$	333	°/s
			$\dot{\delta}_{\min}$	−333	°/s

Acknowledgments

This work was funded by the German Federal Ministry of Economic Affairs and Energy (BMWi) within the "Raudy" project (contract code: 20E1910A) in the national LuFo VI-1 program.

References

[1] Gottfried Sachs. Minimum shear wind strength required for dynamic soaring of albatrosses. *Ibis*, 147(1):1–10, 2005.

[2] Florian Holzapfel. *Nichtlineare adaptive Regelung eines unbemannten Fluggerätes*. PhD thesis, München, 2004.

[3] Peng Lu, Erik-Jan van Kampen, Cornelis de Visser, and Qiping Chu. Aircraft fault-tolerant trajectory control using incremental nonlinear dynamic inversion. *Control Engineering Practice*, 57:126–141, 2016. DOI: https://doi.org/10.1016/j.conengprac.2016.09.010.

[4] S Sieberling, QP Chu, and JA Mulder. Robust flight control using incremental nonlinear dynamic inversion and angular acceleration prediction. *Journal of guidance, control, and dynamics*, 33(6):1732–1742, 2010.

[5] P Smith. A simplified approach to nonlinear dynamic inversion based flight control. In *23rd Atmospheric Flight Mechanics Conference*, page 4461, 1998.

[6] Ezra Tal and Sertac Karaman. Accurate tracking of aggressive quadrotor trajectories using incremental nonlinear dynamic inversion and differential flatness. *IEEE Transactions on Control Systems Technology*, 2020.

[7] Ewoud JJ Smeur, Guido CHE de Croon, and Qiping Chu. Cascaded incremental nonlinear dynamic inversion for mav disturbance rejection. *Control Engineering Practice*, 73:79–90, 2018.

[8] Sungsu Park. Design of three-dimensional path following guidance logic. *International Journal of Aerospace Engineering*, 2018, 2018.

[9] Sanghyuk Park, John Deyst, and Jonathan How. A new nonlinear guidance logic for trajectory tracking. In *AIAA guidance, navigation, and control conference and exhibit*, page 4900, 2004.

[10] Ehab Safwat, Weiguo Zhang, Ahmed Kamel, and Mohamed Kassem. Robustness Analysis of Modified Incremental Nonlinear Dynamic Inversion for Small UAVs. *Automatic Control and Computer Sciences*, 54(2):128–138, mar 2020. DOI: 10.3103/s0146411620020078.

[11] R. A. Sasongko, J. Sembiring, H. Muhammad, and T. Mulyanto. Path following system of small unmanned autonomous vehicle for surveillance application. In *2011 8th Asian Control Conference (ASCC)*, pages 1259–1264, 2011.

[12] Zhiyuan Guan, Hu Liu, Zewei Zheng, Yunpeng Ma, and Tiefu Zhu. Moving path following with integrated direct lift control for carrier landing. *Aerospace Science and Technology*, 120:107247, jan 2022. DOI: 10.1016/j.ast.2021.107247.

[13] Kazuo Tanaka, Motoyasu Tanaka, Yutoku Takahashi, Arimasa Iwase, and Hua O. Wang. 3-D Flight Path Tracking Control for Unmanned Aerial Vehicles Uunder Wind Environments. *IEEE Transactions on Vehicular Technology*, 68(12):11621–11634, dec 2019. DOI: 10.1109/tvt.2019.2944879.

[14] Sungsu Park. A Three-Dimensional Guidance Logic for Continuous Curvature Path Following. *International Journal of Aerospace Engineering*, 2019:1–11, sep 2019. DOI: 10.1155/2019/3754182.

[15] Namhoon Cho, Youdan Kim, and Sanghyuk Park. Three-dimensional nonlinear path-following guidance law based on differential geometry. *IFAC Proceedings Volumes*, 47(3):2503–2508, 2014.

[16] Yi Zhu, Xin Chen, and Chuntao Li. A moving frame trajectory tracking method of a flying-wing UAV using the differential geometry. *International Journal of Aerospace Engineering*, 2016:1–9, 2016. DOI: 10.1155/2016/3406256.

[17] Bartomeu Rubi, Ramon Pérez, and Bernardo Morcego. A survey of path following control strategies for uavs focused on quadrotors. *Journal of Intelligent & Robotic Systems*, 98(2):241–265, 2020.

[18] Peng Lu, Erik-Jan van Kampen, Cornelis de Visser, and Qiping Chu. Aircraft fault-tolerant trajectory control using Incremental Nonlinear Dynamic Inversion. *Control Engineering Practice*, 57:126–141, dec 2016. DOI: 10.1016/j.conengprac.2016.09.010.

[19] Simon P. Schatz and Florian Holzapfel. Modular Trajectory / Path Following Controller Using Nonlinear Error Dynamics. In *2014 IEEE International Conference on Aerospace Electronics and Remote Sensing Technology*. IEEE, nov 2014. DOI: 10.1109/icares.2014.7024374.

[20] Girish Chowdhary, Eric N. Johnson, Rajeev Chandramohan, M. Scott Kimbrell, and Anthony Calise. Guidance and Control of Airplanes Under Actuator Failures and Severe Structural Damage. *Journal of Guidance, Control, and Dynamics*, 36(4):1093–1104, July 2013. DOI: 10.2514/1.58028.

[21] Brian L Stevens, Frank L Lewis, and Eric N Johnson. *Aircraft control and simulation: dynamics, controls design, and autonomous systems*. John Wiley & Sons, 2015.

[22] S. Sieberling, Q. P. Chu, and J. A. Mulder. Robust flight control using incremental nonlinear dynamic inversion and angular acceleration prediction. *Journal of Guidance, Control, and Dynamics*, 33(6):1732–1742, nov 2010. DOI: 10.2514/1.49978.

[23] Ewoud JJ Smeur, Qiping Chu, and Guido CHE de Croon. Adaptive incremental nonlinear dynamic inversion for attitude control of micro air vehicles. *Journal of Guidance, Control, and Dynamics*, 39(3):450–461, 2016. DOI: 10.2514/1.G001490.

[24] Ewoud Smeur, Daan Höppener, and Christophe De Wagter. Prioritized control allocation for quadrotors subject to saturation. In *International Micro Air Vehicle Conference and Flight Competition*, number September, pages 37–43, 2017.

[25] B.J. Bacon, A.J. Ostroff, and S.M. Joshi. Reconfigurable NDI controller using inertial sensor failure detection & isolation. *IEEE Transactions on Aerospace and Electronic Systems*, 37(4):1373–1383, 2001. DOI: 10.1109/7.976972.

[26] Andrew Pressley. *Elementary Differential Geometry*. Springer London, 2010. DOI: 10.1007/978-1-84882-891-9.

[27] Xiuzi Ye and Takashi Maekawa. Differential geometry of intersection curves of two surfaces. *Computer Aided Geometric Design*, 16(8):767–788, sep 1999. DOI: 10.1016/s0167-8396(99)00018-7.

[28] Ola Harkegard. Efficient active set algorithms for solving constrained least squares problems in aircraft control allocation. In *Proceedings of the 41st IEEE Conference on Decision and Control, 2002.*, volume 2, pages 1295–1300. IEEE, 2002.